Eur. Phys. J. A (2013) **49**: 114
DOI 10.1140/epja/i2013-13114-8

THE EUROPEAN PHYSICAL JOURNAL A

Regular Article – Experimental Physics

Measurement of prompt X-rays in ^{238}U(n,f) from threshold to 400 MeV

Investigation of fission charge yield evolution

T. Granier[1,a,b], R.O. Nelson[2], T. Ethvignot[1], M. Devlin[2], N. Fotiades[2], P.E. Garrett[3,c], and W. Younes[3]

[1] CEA, DAM, DIF, 91297 Arpajon, France
[2] Los Alamos National Laboratory, Los Alamos, NM 87545, USA
[3] Lawrence Livermore National Laboratory, Livermore, CA 94551, USA

Received: 25 April 2013 / Revised: 1 August 2013
Published online: 16 September 2013 –
Communicated by N. Alamanos

Abstract. Prompt K X-ray emission yields in the fission induced by neutrons on ^{238}U have been measured for the first time for incident energies ranging from below 1 MeV up to 400 MeV. Results are used to investigate the evolution with incident neutron energy of the fragment elemental distribution and the X-ray emission probability per element. The progressive increase of the symmetric fission probability with neutron energy is observed in qualitative agreement with Wahl systematics for the primary fission fragment charge yields.

1 Introduction

More than seventy years after the discovery of fission, photon spectra associated with fission still are not accurately characterized. X-rays and gamma rays following fission have been studied extensively for spontaneous fission of ^{252}Cf, and thermal neutron-induced fission of ^{233,235}U (see *e.g.* [1–4]). More recently gamma-ray studies have been extended to higher energies for ^{235,238}U [5–8]. However, we know of no comprehensive evaluations of fission photon spectra. Photon emission carries typically about 6% ($\sim$ 3.5% prompt and $\sim$ 2.5% delayed) of the energy released in fission, and the energy deposition, heating and radiation damage produced are different from those due to fission fragments and neutrons. Such X-ray and gamma-ray data, when evaluated and incorporated into libraries, will improve the fidelity of simulations and may be important in better predicting system properties, with applications to power reactors at MeV neutron energies (fast reactor neutron spectra), and at higher energies (tens or hundreds of MeV) for accelerator driven systems for radioactive waste destruction and power generation [9].

Photon emission following fission consists of gamma rays emitted in the de-excitation of the fragments following neutron emission (secondary fragments), X-rays emitted following internal conversion decay of the fragments, and delayed gammas and X-rays following beta decay. In this work we focus mainly on prompt photons, defined as those emitted within $\sim$ 200 ns after scission. Due to nuclear structure and decay properties, the most intense prompt gamma-ray lines correspond to the 2^+ first excited state decay of the even-Z-even-N (even-even) secondary fragments, while the more intense X-rays are associated with states having the largest internal conversion coefficients that tend to be low-lying levels in odd-mass or odd-Z-odd-N (odd-odd) nuclides away from closed shells.

Measurements of prompt fission gamma rays have been performed (see for example, ref. [10]) and provide information on fragment yields for a particular A and Z, when the characteristic gamma-ray energies are known, or if fragments are measured in coincidence with good resolution. However, most of the information obtained is typically for even-even fragments because the best signal to background in the gamma-ray spectrum is for the intense first 2^+ to g.s. transition typical of feeding patterns in even-even nucleus gamma-ray decay. In the case of odd mass or odd-odd fragments, gamma and internal convertion de-excitation involves multiple bands and low-lying levels resulting in a poor signal to background. Thus, the majority of fission gamma-ray data provides information on even-even fragments (see, *e.g.*, refs. [5,7,8,11]).

As discovered over forty years ago, prompt X-rays in nuclear fission originate almost completely in internal conversions associated with prompt gamma de-excitation of the fission fragments [12–14]. Properties of prompt fission X-rays were extensively studied for ^{252}Cf spontaneous fis-

[a] e-mail: thierry.granier@cea.fr
[b] e-mail: granier.th@gmail.com
[c] *Present address*: Dept. of Physics, University of Guelph, Guelph, ON, Canada N1G2W1.

sion and in thermal neutron-induced fission of ^{233}U, ^{235}U and ^{239}Pu [4]. Moreover, the X-ray emission was investigated in ^{235}U fast neutron induced fission for incident neutron energies of 0.7 and 3.5 MeV [15,16]. A review of X-ray emission by fission fragments is given in ref. [17]. Because of their production in internal conversion, the more intense X-ray lines originate with fission fragments that are away from closed shells and are often odd mass or odd-odd nuclides. Thus X-rays tend to sample a different subset of fission fragments than gamma rays, and their yields are very dependent upon nuclear structure of the fragments produced.

The present work aims at extending investigations of prompt fission X-rays to higher incident neutron energies. For the first time prompt K X-ray yields in ^{238}U(n,f) have been measured for incident neutron energies ranging from 1 to 400 MeV. The results provide interesting information on fragment de-excitation which will be useful for constraining phenomenological or semi-phenomenological models of fission. Also, although prompt X-ray yields are not a measure of the fission fragment charge yields they can be used to infer the fission fragment charge distribution evolution as a function of incident neutron energy.

This study is part of a collaborative effort on nuclear fission research by teams of the Commissariat à l'Énergie Atomique in Bruyères le Châtel and the Los Alamos Neutron Science Center. In this framework, measurements of prompt fission neutron energy and multiplicity [18–20] and on prompt fission gamma-ray emission [6–8] have been performed these last years. Preliminary results of this study were included in an IAEA report on fission product yield data [8].

2 Experiment

The experiment was conducted at the WNR facility of the Los Alamos Neutron Science Center (LANSCE) [21, 22]. It was based on the GEANIE array of photon spectrometers [23,24] and a dedicated ^{238}U active target which permitted detection of fission events with a high efficiency. GEANIE is located on the 60 degree right neutron flight-path of WNR at a distance of 20.34 meters from the neutron production target. The neutrons were produced through spallation induced by 800 MeV protons emitted in sub-nanosecond pulses every 1.8 μs. This temporal structure is well suited for measuring the incident neutron energy using the time-of-flight technique. The ^{238}U active target was centered in the detector array into the collimated neutron beam trajectory. Most of the time, when a fission occurred in the target, it generated a signal. This signal was used to trigger the data acquisition system which then collected the signals from the photon detectors in coincidence. The time delay between the fission signal and the proton beam-pulse timing signal was also recorded. This time delay corresponds to the time of flight of the incident neutron and this information was used off-line to compute the corresponding kinetic energy. In this way photon energy spectra are obtained for groups of incident neutron energies.

The fission target consisted of eight 1 mg/cm^2 thin layers of high-purity ^{238}U, each deposited onto a photovoltaic (solar) cell by a mass separator. The total mass of ^{238}U in the target was about 25 mg. Each solar cell is an independent detector able to detect one of the fission fragments from a fission event occurring in the associated ^{238}U layer with a high efficiency ($\gtrsim$ 80%). The precise knowledge of the efficiency was not required in the experiment because fission detection was used only as a trigger. The solar cells were operated with SAPHiR charge preamplifiers [25]. With these preamplifiers the time resolution for fission detection was about 8 ns (FWHM). Fission-induced signals from the solar cells were easily discriminated from alpha-induced signals and noise. This fission target was designed to minimize the attenuation of low-energy photon radiation. Although the solar cells can exhibit decreased efficiency due to alpha particle damage, the alpha flux from ^{238}U (and ^{235}U in another experiment) was small enough that no noticeable loss of efficiency occurred during the course of the experiment. Damage from exposure to the high-energy neutron beam also was not seen in the course of these experiments. The fission fragment detector is described in detail in ref. [26].

Resolution achieved on the incident neutron energy is mainly driven by the time resolution of the fission detector. The neutron energy resolution was determined from the time width of the spallation target gamma flash to be 1% at 1 MeV, 3.3% at 10 MeV and 10% at 100 MeV incident neutron energy.

Neutron fluence on target integrated up to 30 MeV neutron energy was on the order of 10^6 neutrons s^{-1}cm^{-2}. The neutron energy spectrum was basically a classical spallation spectrum, slightly modified by the presence of 1.5 cm lead and 2.5 cm borated polyethylene attenuators in the beam. These attenuators were respectively designed to diminish the intensity of the gamma-flash induced by the spallation reactions and the flux of low-energy, scattered neutrons.

GEANIE was comprised of 26 high-resolution germanium (Ge) gamma-ray detectors, twenty of which were equipped with bismuth germanate background suppression shields. Eleven of the shielded Ge detectors were planar detectors dedicated to low-energy photon spectroscopy, typically, from $\sim$ 10 keV up to 300 keV (but with spectra extending to 1 MeV).

About nine million fission-photon coincidences were recorded at a rate of $\sim$ 15 per second using the whole array. Most of these data correspond to fission gamma rays. Thick sample experiments provide even more gamma rays and these were exploited in refs. [5,7,8]. About 5% of these coincidences correspond to X-rays emitted in fission and were analyzed in the present work.

3 Detector characteristics

Calibrated radioactive point-like sources of ^{252}Cf, ^{241}Am and ^{133}Ba were used to calibrate the low-energy photon detectors in the relevant energy region as well as to measure their resolution as a function of photon energy.

The typical resolution achieved was 0.6 keV (FWHM) at 30 keV. However, some of the LEPS detectors had a slightly degraded resolution because of neutron radiation damage effects. These data were also used to determine the efficiency response of each detector. The five best detectors in terms of resolution and efficiency were retained for the analysis. Due to the large value of the resolution compared to the intrinsic widths of the K X-ray lines [27], the lineshape of each individual X-ray line observed in the spectra is Gaussian to a good approximation.

Although the target was designed to minimize X-ray attenuation, this phenomenon remains large at low energy and needs to be corrected for. To study this effect Monte Carlo simulations were realized with the code MCNP4C2 [28]. The target geometry and constituting materials were precisely described. This included the silicon and silver backings of the photovoltaic cells as well as the target holder made of plastic. Also, the positions of the germanium detector were described. The corresponding X-ray transmission averaged over the eight deposited cells ranges from about 20% for 12 keV X-rays (light fragments) to 70% for 35 keV X-rays (heavy fragments). These values were found to be consistent with experimental data recorded with a low-energy photon source placed in different configurations behind the target in the field of view of the detectors.

Parametrisations describing the variation as a function of photon energy of the efficiency, the resolution and the photon transmission were obtained and used subsequently in the analysis of the fission prompt photon spectra.

4 Spectra characteristics

Photon energy spectra were produced off-line by requiring a 200 ns time coincidence between photon and fission signals. This value is consistent with the slow rise time at low energy inherent to the Ge detectors and takes into account imperfections in the time alignment of the different photon detector channels. The choice of a 200 ns time gate defines the time range for observation of "prompt" fission X-rays. X-rays from states with half lives much longer than this will appear as part of the time-random background spectrum.

There is no evidence of Doppler shift or broadening in the X-ray spectra. Based on measurements of K X-ray emission times for fission fragments reported in ref. [13] and the stopping of fragments in our setup, to a very good approximation, all fragments are stopped and neutral when X-rays are emitted. Thus neither Doppler effects, nor the expected 900 eV energy shift [11] expected of X-rays from ionized fragments are expected to influence our results.

The fission prompt K X-ray spectra are quite complex since they are comprised of five X-ray lines per element. However, the energies and relative intensities of these lines are known to a high precision [29]. These five lines are arranged in a doublet, $K_{\alpha_{1,2}}$, and a typically five times less intense triplet, $K_{\beta_{1,2,3}}$, located 1 to 5 keV higher in energy depending on Z. In addition, a continuous background

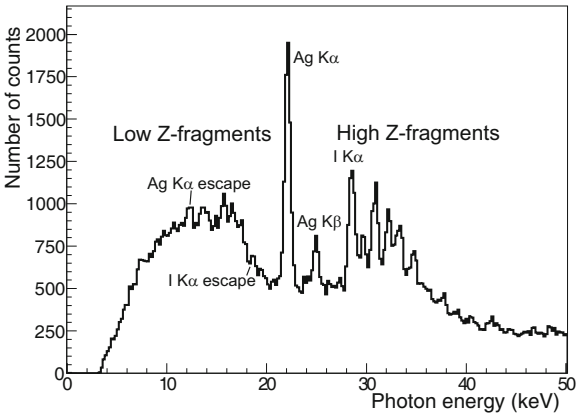

Fig. 1. Low-energy photon spectrum in coincidence with neutron-induced fission for incident neutrons energies between 0.7 and 6 MeV ($\bar{E}$ = 3 MeV). Fission fragment K X-rays are visible and the overall shape of the X-ray spectrum reflects the expected charge asymmetry characteristic of fission at this energy. Note that the intense Ag peaks are due to an experimental artifact.

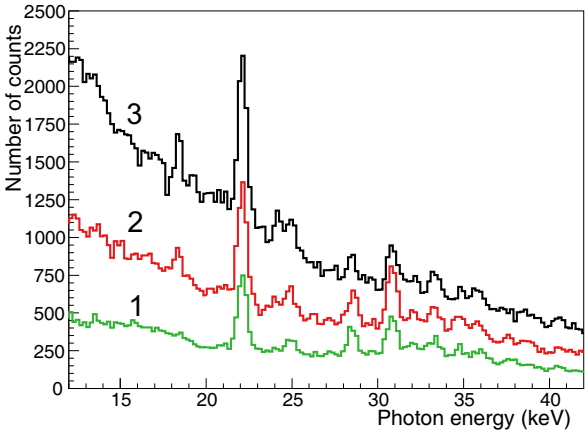

Fig. 2. Evolution with increasing incident neutron energy of the photon energy spectrum in the 12–42 keV region. 1) 12–17 MeV, $\bar{E}$ = 14 MeV; 2) 17–50 MeV, $\bar{E}$ = 32 MeV; 3) 50–400 MeV, $\bar{E}$ = 180 MeV.

is observed below the peaks. This background is due to random coincidences and coincidences with Compton tails of fission γ-rays.

At low incident neutron energy, where fission induced on ^{238}U is known to be preferentially asymmetric, the fission prompt K X-ray spectrum is mostly populated within two regions of photon energy (see fig. 1). A low-energy region extending roughly from 5 to 20 keV corresponds to the light ($28 \lesssim Z \lesssim 45$) fragments and a higher energy region from about 25 to 40 keV corresponds to the heavy ($51 \lesssim Z \lesssim 61$) fragments. At higher neutron energy, this figure is modified since the contribution from symmetric fission increases (see fig. 2).

Another well-known property observed is the odd-even effect in Z favoring X-ray production for odd nuclear charges. This effect is attributed to a larger amount of internal conversions because of the larger number of low-lying excited states in the odd-odd and odd-mass nuclei.

Another feature observed is an intense peak corresponding to the Ag K_α doublet. The intensity observed far exceeds the production of Ag fission fragments and is explained by γ-induced fluorescence in the silver backings of the solar cells. Due to the relatively large thickness of these backings, the amount of real and chance coincidences of fluorescence X-rays with fission is high. To a lesser extent, L X-rays from uranium excitations are also visible in the spectra.

Also, some peaks corresponding to the escape of Ge K X-rays can be observed. This phenomenon is well known in photon spectroscopy below 50 keV with Ge detectors and is described for example in ref. [30]. Subsequent to the photoelectric absorption of the primary radiation in the Ge crystal, Ge K X-rays originating from the atomic shell rearrangement after the photoelectron emission can escape the crystal and contribute to secondary peaks located about 10 keV below the full energy peak. In fig. 1 the escape peaks associated with the silver and iodine K_α peaks can be observed.

5 X-ray analysis

X-ray yields have been extracted for the following bins of incident neutron energies: 0.7–6 MeV, 6–11 MeV, 11–20 MeV, 20–50 MeV and 50–400 MeV. This wide binning was driven by statistical considerations. Since the low energy photon detection threshold was about 12 keV for some of the germanium detectors, the spectrum analysis was restricted to the 12–45 keV region.

The spectrum analysis has been performed using a dedicated suite of programs developed under the PAW software from CERN [31]. These programs were coupled to an X-ray data base and made use of the MINUIT program for function minimization and error analysis [32]. The spectral background below the peaks was determined automatically via the method proposed by Westmeier [33, 34], which has the advantage of describing satisfactorily the steplike baseline shape under photoelectric peaks [30].

The following procedure was conducted to deconvolute the X-ray spectra. In a first pass, background below X-ray peaks was determined by the program. The spectrum was then background-subtracted while preserving the original statistical uncertainty associated with each spectrum channel.

Least squares fit of the background-subtracted spectrum was then performed with a parametric function describing the different X-ray contributions. The function consists of a weighted sum of Gaussians, each Gaussian describing a given X-ray line. All X-ray lines, corresponding to fission fragments and uranium excitations, which may lie in the considered energy range are taken into account. Also, the Ge K X-ray escape peaks associated with the most prominent full energy peaks have been included. X-ray line energies are fixed according to X-ray standards [29]. The width of the Gaussians is fixed according to the systematic variation of the detector resolution as a function of photon energy which has been studied with calibrated radioactive sources. The intensity of the escape peaks is fixed relative to that of the corresponding full energy peak in the following way: the intensity ratio between the full energy peak and the escape peak has been measured for Ba K_α peaks using data recorded with a ^{133}Ba calibrated X-ray source. The variation of the intensity ratio with photon energy is then taken from X-ray spectroscopy literature [35], so that the relative intensity of the escape peaks can be fixed for all relevant full energy peaks. In addition, each photon line is attributed a weight accounting for detection efficiency and photon transmission at the corresponding energy as obtained from the systematic studies. Lines belonging to the same element are attributed relative weights according to X-ray standards [29].

Finally, although the fitted function describes a large number of photon peaks, it includes only a limited number of free parameters, only one per element. This number remains small compared with the number of data points in the spectra. Examples of deconvoluted X-ray spectra are displayed in fig. 3. They correspond to incident neutron energies lying between 0.7 and 6 MeV. The photon spectrum between 20 and 41 keV (bottom panel in fig. 3) has been fitted with a function describing 90 X-ray peaks with 18 free parameters corresponding to 18 elements.

The statistical uncertainty associated with each spectrum channel was taken into account in the minimization procedure. In practice, two sections of the spectrum, partially overlapping, were successively fitted (typically 11–23 keV and 20–42 keV). The results of the low-energy fit were used as initial values for the high-energy section fit for the elements common to both sections.

In some cases the fit obtained in the first pass was not satisfactory in describing local minima in the spectrum. This was in particular the case for unresolved regions such as the 30–36 KeV range. A second pass was then initiated with some corrections on the background shape previously determined automatically. Particular attention has been paid to keep the background estimate as smooth and simple as possible. The uncertainty on the final results due to background determination is discussed in the next section.

The χ^2 values resulting from the fits remain between 0.6 and 1.8. This indicates the good quality of the fits and that the number of free parameters was not too large with respect to the information contained in the spectra. The uncertainties associated with the fitted parameters are obtained by making use of the MINOS processor from the MINUIT package which takes into account parameter correlations and non linearities [32]. They are used to compute the uncertainties of the K X-ray yields.

6 Systematic uncertainty

The systematic uncertainties of the measurement can be divided into instrumental and analytical. The main sources of instrumental systematic errors are the uncertainty on photon detection efficiency and X-ray transmission correction. The uncertainty on detection efficiency is related to that of the activities of the radioactive sources and has been estimated to be about 3%. The uncertainty

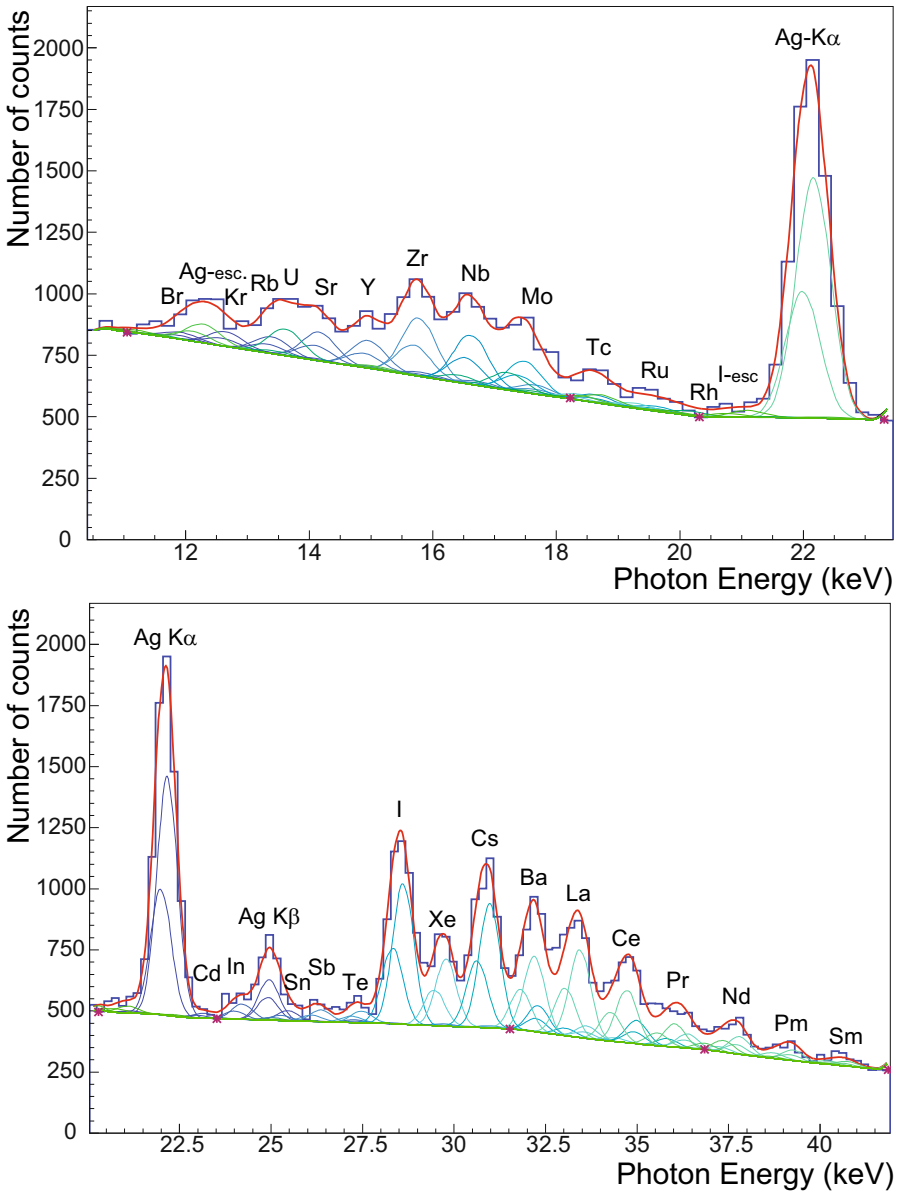

Fig. 3. Example of spectrum deconvolution in terms of X-ray lines. Top: 10–23 keV region. Bottom: 20–41 keV region. The main peaks are labeled. Incident neutron energy is from 0.7 to 6 MeV corresponding to $\bar{E} = 3$ MeV. Although the number of X-ray lines taken into account is large, the number of free parameters in the fitting procedure remains limited to one per element.

on photon attenuation which is based on a Monte Carlo simulation is estimated to be about 7%, giving an overal uncertainty of $\sim 10\%$ on the final results due to both corrections. Also, as mentioned earlier, fluorescence induced in the silver constituting the photovoltaic cell backings results in a significant enhancement of the silver K X-ray peaks. Since this effect cannot be discriminated from the Ag X-ray production in fission, this element has been removed from the final results.

The analytical systematic uncertainty is certainly dominated by the uncertainty on background determination. This uncertainty is directly related to the peak to background ratio. It is moderate for an intense, well-resolved peak whereas it can be large for a small, partially resolved peak. The sensitivity to background determination has been studied by deconvoluting the spectrum with both artificially lowered and enhanced background assumptions. In doing so the resulting fit was significantly degraded. Upper and lower limits of the background models were determined on this basis. In order to assess an uncertainty in terms of a Gaussian width, sigma, we have considered these upper and lower background limits as 3-σ deviations from the background model of our best fit considered as the best determination of the real background shape. Under this assumption, the 1-σ uncertainty associated with background remains most of the time on the order of 10%, in particular for $Z = 40$–42 and $Z = 50$–56. However, it becomes large (50% and above) for the less prominent X-ray peaks such as those corresponding to symmetric fission ($Z = 43$–49).

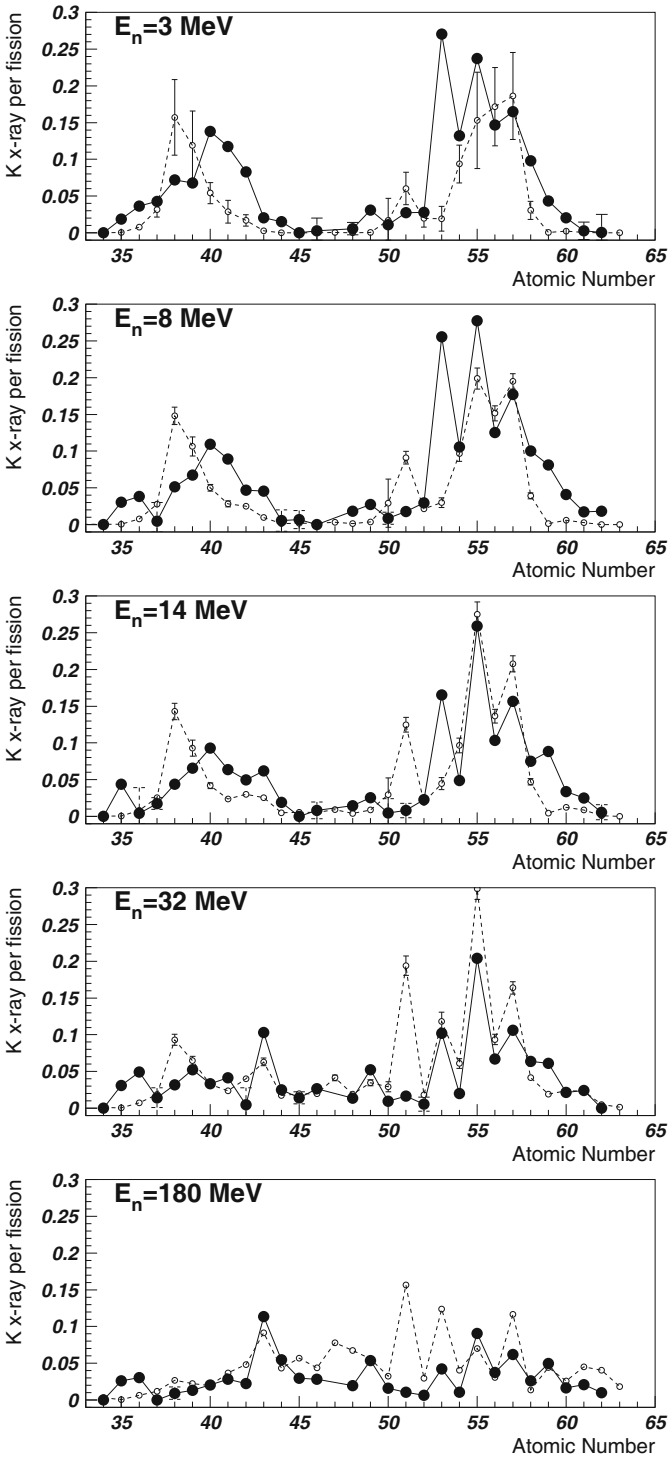

Fig. 4. K X-ray yields per fission for five bins of incident neutron energies. Solid dots: this experiment. Open dots: calculations (see text).

7 Results on X-ray yields

The results for the K X-ray yields per fission are listed in table 1 and represented in fig. 4 for five bins of incident neutron energies (E_n): 0.7–6 MeV, 6–11 MeV, 11–20 MeV, 20–50 MeV and 50–400 MeV. The corresponding average energies are respectively 3, 8, 14, 32 and 180 MeV. These data correspond to the sum of K_α and K_β rays of each element per fission.

The trend already visible in fig. 2 is confirmed here. The X-ray yields follow the trend expected for the charge yields. This is more clearly visible in fig. 5 which displays the evolution as a function of E_n for 3 groups of elements respectively situated in the light peak, symmetric region and heavy peak of the fission fragments. The main feature here is the expected enhancement of the symmetric fission probability, whereas the probability for asymmetric fission decreases.

Examination of the data features shows the expected greater X-ray yield from odd-Z nuclei, for example Nb, Cs, I, La, although some even-Z nuclei such as Zr and Mo have large yields. Large X-ray yields for Zr were seen similarly in spontaneous fission of ^{252}Cf [11]. We note, as an example of nuclear structure affecting the X-ray yields, that the X-ray yield from Y will be reduced in our measurement due to the delayed decay (8.6 μs) of one of the highly converted levels in ^{99}Y.

8 X-ray yield calculations

Detailed calculations of X-ray yields were performed on the basis of two main ingredients: 1) the Wahl systematics for fission product yields for ^{238}U(n,f) [36], 2) up-to-date data on level schemes (*i.e.* branching ratios and internal conversion coefficients) [37] for the secondary fission fragment nuclides. In order to compare with the measurements, Wahl systematic yields have been calculated for the five incident neutron energy bins given above using the CYFP code [38]. Among other features, this code computes the isotopic fission yields for neutron-induced fission of actinides at a given incident neutron energy. Since the energy intervals were broad, the yields were calculated for several neutron energy values within each energy interval. Then, these results were averaged within each interval using weights reflecting the energy spectrum of the incident neutrons as obtained from the experimental time-of-flight data. The uncertainties given by CYFP were also propagated in this process. It was observed that in some cases the uncertainty provided by CYFP is quite large, even though the yields are substantial. This was observed in particular for ^{130,131,132}Sn, ^{132,133}Sb, ^{133,134}Te, and ^{135}I for some neutron energies below 6 MeV. These divergences are also present in the CYFP-based UKFY4.1 library of fission product yields [39]. They are most likely due to numerical problems in the CYFP code and it was chosen to allocate a realistic value for the uncertainty in those cases. This value was chosen to be equal to that of neighboring isotopes with similar fission yields or to the uncertainty given by the code for the same isotope but at a different incident neutron energy for which the numerical problem is not seen.

For each isotope with non-negligible production, level scheme data from ref. [37] were used to calculate the amount of internal conversion in the prompt gamma decay process from the internal conversion coefficients and

Table 1. K X-rays per fission $Y_k(Z)$ for 5 bins of incident neutron energies (see text). u(Y_K) is the relative uncertainty in percent as derived from the fits.

	Thresh.–6 MeV		6–11 MeV		11–20 MeV		20–50 MeV		50–400 MeV	
Z	Y_K ($\times 10^5$)	u(Y_K) (%)	Y_K ($\times 10^5$)	u(Y_K) (%)	Y_K ($\times 10^5$)	u(Y_K) (%)	Y_K ($\times 10^5$)	u(Y_K) (%)	Y_K ($\times 10^5$)	u(Y_K) (%)
35	5920	42	9620	41	13850	34	9870	34	8240	35
36	14510	22	15270	32	1590	354	19650	22	12120	34
37	15920	26	1720	257	6480	80	5290	133	0	0
38	21540	11	15430	22	13030	31	9480	33	2750	84
39	13420	11	13290	17	12960	20	10310	18	2600	50
40	21770	6	17250	10	14670	14	5250	25	3240	33
41	12230	7	9260	12	6610	19	4300	26	2940	26
42	10090	10	5720	21	6060	23	530	236	2720	35
43	1410	28	3150	20	4260	18	7110	9	7810	7
44	1760	36	660	144	2210	52	2890	29	6380	11
45	0	0	660	124	0	0	1360	84	2880	18
46	450	171	440	1730	1240	115	4020	25	4270	21
48	790	85	2560	43	2070	57	1970	43	2760	33
49	5690	15	4980	22	4640	35	9540	12	9840	11
50	11060	46	8730	81	4760	193	9610	62	15950	36
51	5690	15	3700	26	1700	97	3460	33	2230	48
52	14230	15	15050	22	11530	35	2750	95	3290	78
53	18360	2	17360	3	11210	6	6940	6	2890	12
54	25770	4	20570	6	9490	16	3950	20	2080	44
55	13330	2	15570	3	14560	4	11470	3	5090	6
56	10300	3	8790	6	7260	8	4710	7	2630	13
57	6590	3	7090	5	6260	6	4250	5	2470	8
58	3880	5	3970	7	2970	10	2530	8	1030	17
59	1020	10	1920	8	2100	9	1440	8	1180	8
60	310	19	610	15	500	20	320	19	250	24
61	50	120	300	30	430	26	420	19	360	19
62	10	200	250	28	80	100	0	0	140	36

gamma-ray intensities. Most of the converted gamma transitions initiate from isomeric levels with half lives not always negligible with respect to the 200 ns measurement windows. To properly account for their contribution, a lifetime factor was applied. This factor varies from 1.0 for prompt photons (no correction) to essentially zero (no contribution) for long-lived states.

The fission K X-ray yields were obtained by multiplying the obtained amount of converted transitions by the isotopic fission yields and by the 1984 evaluated X-ray fluorescence yields of Bambynek [40], and then summing over isotopes of each atomic number. Full population of the isomeric states per fission is assumed in the calculation, although this is certainly not true in all cases. The resulting calculated X-ray yields as a function of Z are represented in fig. 4 together with the measured yields. It can be seen that the agreement with the measurements is fair overall and excellent for some Z values. However, there are cases where measurement far exceeds calculation, suggesting that some highly converted transitions are missing in the level scheme data. The lack of information in level schemes is evident, for instance, in the heavier isotopes of iodine ($Z = 53$) for which only very few levels are currently known. We observe that the discrepancy between measurement and calculation, on average, progressively decreases as the incident neutron energy increases. This is because, at higher energies, the mass distribution of the fragments for a given Z is shifted towards lower masses,

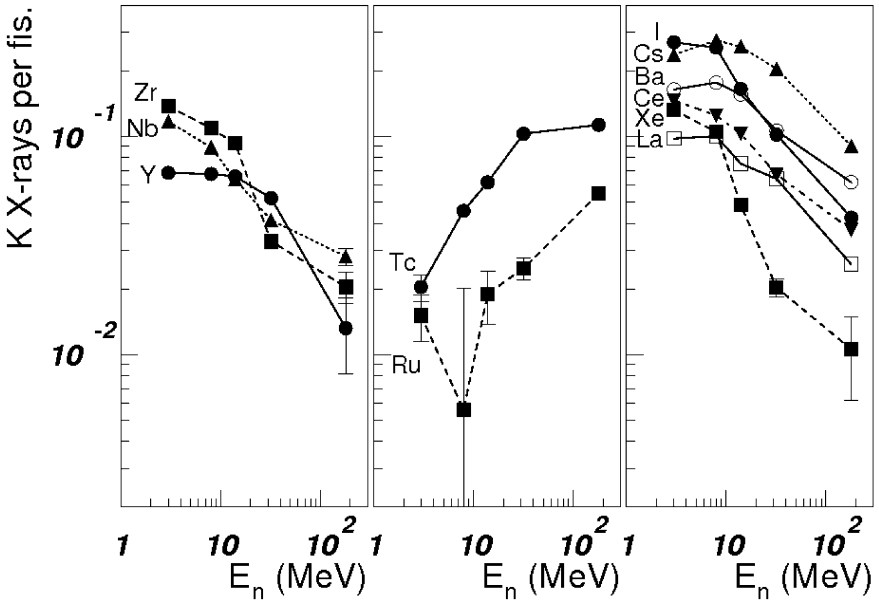

Fig. 5. Evolution of K X-ray yields as a function of E_n for a selection of elements corresponding to light (left panel), intermediate (central panel) and heavy (right panel) fragments.

i.e. more stable nuclei, for which level scheme data are much more complete. In contrast, in the case of Sb, calculations and measurements agree at lower energies, whereas calculations exceed measurements as energies get higher, with an increasing mismatch. This behavior suggests that at higher energies there may be a shift to nuclei in which prompt (200 ns) gamma decay may involve blocking isomeric states or opening of pathways which bypass low-lying strongly converted transitions, in contrast to our assumption of 100% population. These results provide an indication of nuclei in which to search for internally converted states that decay on a 200 ns time scale via predominantly $E2$ and $M1$ transitions.

9 Investigation of fission charge yields

The question naturally arises whether prompt K X-ray yields can be used to assess fission charge yields quantitatively.

Since the prompt K X-rays are emitted subsequently to the internal conversions occurring in the prompt de-excitation of the fission fragments, their yields are necessarily related to fission charge yields. For given A and Z, the average number of K X-rays emitted per fission, or $Y_K(Z,A)$ is the product of the isotopic yield $Y(Z,A)$ by the average number of K X-rays emitted per fragment during their prompt de-excitation $K(Z,A)$,

$$Y_K(Z,A) = Y(Z,A) \cdot K(Z,A)\,. \tag{1}$$

Summing over A, eq. (1) can be rewritten,

$$Y_K(Z) = Y(Z) \cdot K(Z)\,, \tag{2}$$

where $K(Z)$ is the mean K X-ray emission probability per fragment of element Z.

We note that the values of $K(Z,A)$ depend on the internal conversion decay properties of each nuclide. If the feeding and decay of these levels were well known, then the values of $K(Z,A)$ could be calculated, however, lack of knowledge of the internal conversion coefficients, lifetimes and even energies for many of the levels make this task difficult and not very accurate in many cases as shown in the preceding section.

The K X-ray emission probability was studied by Reisdorf *et al.*in the early seventies [4] in low-energy fission of several actinides. In this early work coincident measurements of the kinetic energies of both fragments and the prompt K X-rays were performed. $K(Z)$ was obtained for spontaneous fission of ^{252}Cf and in thermal neutron-induced fission of ^{233}U, ^{235}U and ^{239}Pu. The K X-ray emission probability was found to vary systematically with Z and A for all the studied systems following a sawtooth curve (fig. 6). It is at a minimum at low Z and A ($Z = 36$, $A = 90$) then increases with increasing Z and A to reach a plateau at $A \simeq 108$, $Z \simeq 42$, then drops for $Z > 48$ and increases again up to $Z = 61$, $A = 156$ where it reaches a plateau. This behavior is interpreted in terms of transition from sphericity to deformation when going away from closed shells ($N = 50, 82$, $Z = 82$). The transition from pure vibrational to rotational excited states is reflected in the increasing number of low-energy γ transitions in the de-excitation of the fragments, favoring internal conversions.

Another interesting finding of ref. [4] is that $K(Z)$ does not vary strongly from one system to another. This is illustrated in Fig. 6 where the ratios of $K(Z)$ for ^{233}U(n,f), ^{239}Pu(n,f) and ^{252}Cf to $K(Z)$ for ^{235}U(n,f) are also represented. It can be seen that for all systems the ratio remains in a 50% envelope for almost all Z values.

Obviously in the present case the fissioning system differs from those investigated by Reisdorf. Depending on incident neutron energy and the opening of the different emission channels prior to fission, the fissioning system is possibly ^{239}U (first chance fission), ^{238}U (second chance fission), but also lighter isotopes of U and even isotopes of Th and Pa. Moreover, Reisdorf's results were obtained at low excitation energy whereas in the present case higher excitation energies and spin are expected for the fissioning system.

However, there are several factors that tend to make X-ray emission following fission vary slowly with changing incident neutron energy:

1) Post neutron fragment excitation varies little with incident neutron energy. Neutron emission takes much of the available energy from the fissioning system with the average number of emitted neutrons increasing rapidly with increasing neutron energy, and pre-equilibrium neutron emission potentially removing a large fraction of the incident energy at high energies [20]. Recent measurements of prompt fission neutron spectra in ^{238}U(n,f) for incident neutron energies from 1 to 200 MeV indicate that the increase of fragment temperature remains slight over this entire incident neutron energy range [18]. Although, average total gamma-ray energy emitted does increase by about 2 MeV over the indicent neutron energy range from thermal to 20 MeV (see ref. [41] and references therein).
2) For the heavier-mass fragment peak there is almost no shift in fragment masses with increasing E_n, only broadening of the peak is observed. There is a shift to lower masses, however, for the lighter mass fragments with increasing incident neutron energy.
3) Nuclear level structure of isotopes differing by only 2 neutrons is often similar so that internal conversion rates may be similar as well, although large variations in conversion may occur.

Following these arguments it is instructive to use Reisdorf's measurements as a prescription for $K(Z)$ in order to infer fission charge yields from our measurements. Although this may be a crude approximation, the order of magnitude of the error made can be estimated from the spread on $K(Z)$ observed for the different fissioning systems in fig. 6.

The charge distributions obtained in this way are displayed in figs. 7–9. The values of $K(Z)$ were taken from the measurements for ^{235}U(n,f) when available and otherwise from that for ^{252}Cf spontaneous fission.

It must be stressed that the data in figs. 7–9 are absolute. No normalization has been applied. Two error bars are represented, corresponding to the uncertainty derived from the least squares fits (solid bar) and the quadratic addition of this latter with the 50% relative uncertainty associated with the $K(Z)$ values (dotted bar).

The first observation is that the shapes of the charge distributions correspond well to the expectations of a progressive increase of the symmetric fission probability with a decrease of the asymmetric one, as well as an overall

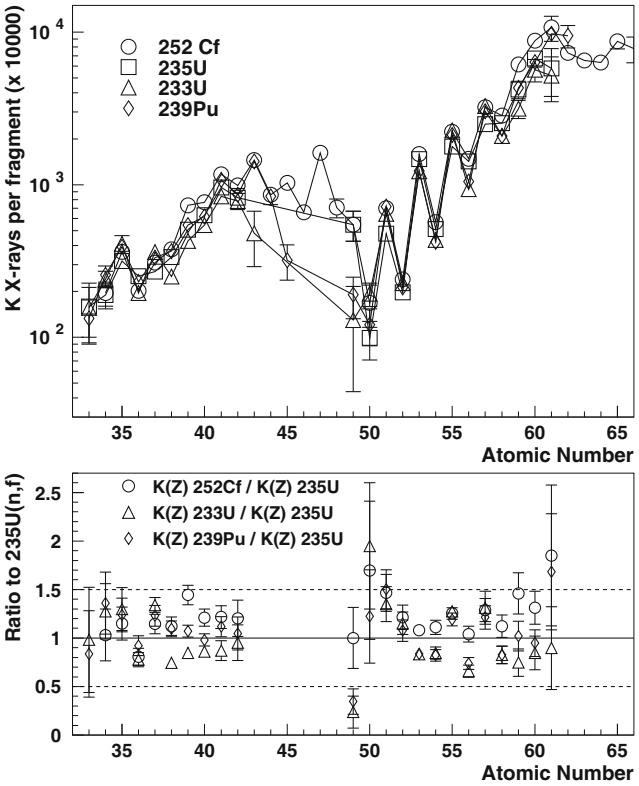

Fig. 6. Top: Mean K X-ray emission probabilities per fragment of charge Z ($K(Z)$) obtained by Reisdorf *et al.* [4] for ^{252}Cf spontaneous fission (circles), ^{235}U(n,f) (squares), ^{233}U(n,f) (triangles) and ^{239}Pu(n,f) (diamonds). Bottom: Ratio of $K(Z)$ in ^{252}Cf spontaneous fission (circles), ^{233}U(n,f) (triangles) and ^{239}Pu(n,f) (diamonds) to $K(Z)$ for ^{235}U (data from ref. [4]).

broadening. These results follow the progressive transition towards symmetric fission reported in ref. [42] for measured fission mass yields in ^{238}U(n,f).

The results for the first four energy intervals have been compared with model calculations using the GEF code (version 2013/1.7) [43]. The calculations were performed for the mean energy of each energy interval, *i.e.* 3, 8, 14 and 32 MeV, respectively. It was not possible to compute the charge yields for the highest energy bin with this code. As can be seen in figs. 7 and 8, the agreement of the GEF calculation with our results is quite good for the four energy bins.

In the same figures the results are also compared with the Wahl systematics determined for the corresponding energy intervals (see previous section). The Wahl systematics are represented with the associated uncertainty (hatched areas). The agreement is also surprisingly good for all energy intervals. This seems to confirm that $K(Z)$ does not vary strongly when going to higher incident energies.

The agreement with Wahl is slightly degraded for the higher energy interval ($\langle E_n \rangle = 180$ MeV), where the obtained charge yields seem to be, for the most part, systematically lower than the Wahl systematics. This can be

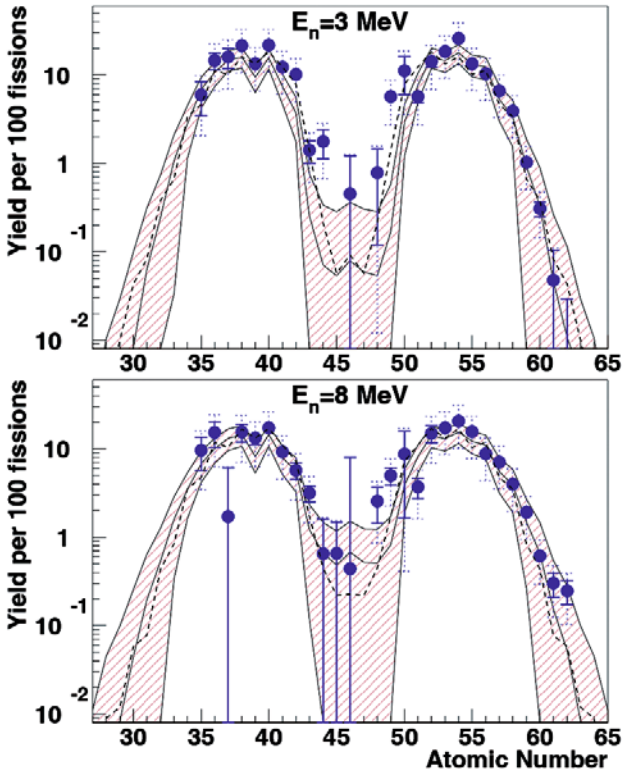

Fig. 7. Charge distributions determined from the X-ray yield measurements (symbols). Top: threshold–6 MeV, $\langle E_n \rangle \simeq 3$ MeV. Bottom: 6–11 MeV, $\langle E_n \rangle \simeq 8$ MeV. Solid error bars correspond to propagated fit errors, dotted error bars correspond to the sum in quadrature of the fit error and the 50% relative uncertainty associated with $K(Z)$. Dashed curve is the result of the GEF code by Schmidt-Jurado [43] (see text). Solid curve within hatched area corresponds to Wahl systematics and associated uncertainty obtained for the corresponding energy ranges.

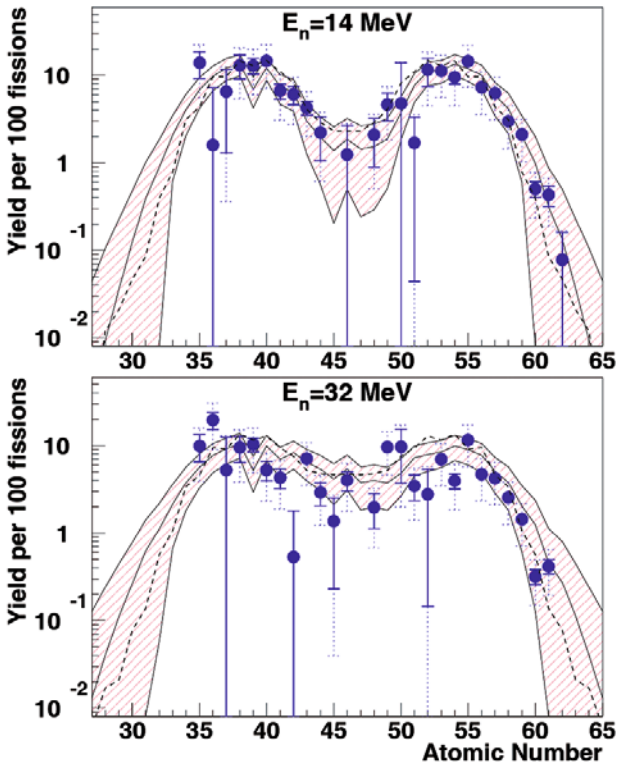

Fig. 8. Same as fig. 7. Top: 11–20 MeV, $\langle E_n \rangle \simeq 14$ MeV. Bottom: 20–50 MeV, $\langle E_n \rangle \simeq 32$ MeV.

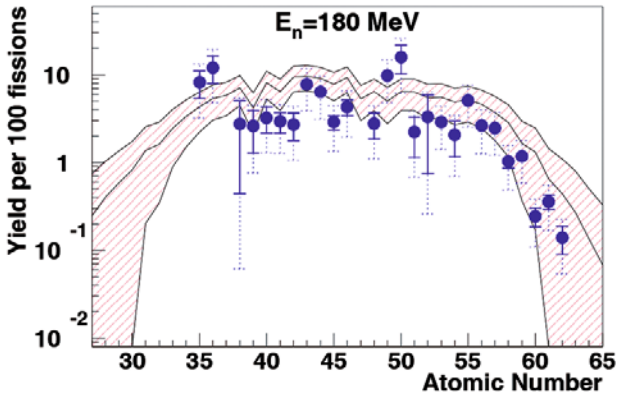

Fig. 9. Same as fig. 7 for 50–400 MeV incident neutron energy interval, $\langle E_n \rangle \simeq 180$ MeV.

interpreted, at least partly, as a decrease of the average radiation probability $K(Z)$ due to the shift towards lower masses in the fragment mass distribution at given Z, presumably with lower internal conversion rates on average. In refs. [6,7], a typical mass shift of 4 to 5 mass units is reported when going from $E_n = 3$ MeV to $E_n = 70$ MeV in the Z domain from 50 to 60. According to the systematic variation of the K X-ray emission probability with A reported in ref. [4], one might expect a decrease of $K(Z)$ by at least a factor of 2. The same behavior is also expected in the Z domain from 36 to 41. This correction on the radiation probability would improve the agreement of the obtained charge distributions for high incident neutron energies with the Wahl systematics.

One could conceive a study in depth to determine $K(Z)$ through the modeling of the de-excitation of each isotope, taking into account the mass shift with increasing energy. However, as stated above, the level schemes of most fission fragments are not well known, particularly for the most converted transitions whose contribution to $K(Z)$ is the highest. Thus such a determination of $K(Z)$ would have to rely on models to a large extent. The recent development of Monte Carlo models of nuclear fission (see, *e.g.*, refs. [44–49]) can provide tools to investigate this quantity provided internal conversion models are implemented in the simulation of the fragments de-excitation. Conversely, the present X-ray data provide an additional test for these models.

Alternatively, coincidence measurements of X-rays with conversion electrons and gamma rays can determine the nuclear levels from which the X-rays originate as demonstrated by Watson *et al.* [11]. With the LANSCE neutron source and GEANIE array, fission detectors

with a larger amount of fissionable material are needed to enable such studies.

To summarize, two main conclusions can be drawn from this study of the variation of the K X-ray emission probability as a function of incident neutron energy. First, the variation remains moderate even over our large incident neutron energy range. This has been explained in part through the changes in neutron emission that tend to keep fragment excitations independent of incident neutron energy. Second, X-ray emission appears to be dominated by the transition of the nucleonic composition of the post neutron fragments toward smaller numbers of neutrons. Presumably these lighter fragments, on average, have reduced internal conversion because they are getting closer to closed-shell nuclei.

10 Conclusion

Measurements of prompt K X-ray yields in ^{238}U(n,f) have been performed for the first time for fast neutron energies ranging from 0.7 MeV to 400 MeV. These data provide integral information on fission fragment de-excitation which may be useful for modeling nuclear fission for applications and for basic understanding. Corresponding fission fragment charge distributions have been derived from these data using K X-ray emission probabilities per fragment obtained in an earlier work in low-energy fission [4].

Results are in good agreement with GEF model calculations [43] and Wahl systematics [36,38] and corroborate, at least qualitatively, the evolution of the mass distribution measured in another work [42] for the same system. This shows that the K X-ray emission probability $K(Z)$ is not strongly changed at higher incident neutron energies despite different nucleonic composition, excitation energies and spins of the fragments. The main influence on $K(Z)$ seems to be due to the shift towards lighter mass fragments and more symmetric fission with increasing incident neutron energy.

Measurements of X-ray and gamma-ray coincidences can provide more detailed information on the production, excitation and level properties of individual fragments, however, greater statistics are needed for such studies. Extension of these measurements to more alpha active materials will require the use of alternate fission fragment detectors such as gas-filled counters where radiation damage is not an issue.

These data provide new information on the low-energy portion of the photon spectrum emitted in neutron-induced fission of ^{238}U for a very wide range of incident neutron energies. Such data are complementary (both in photon energy range and in arising more from odd-mass and odd-Z-odd-N fragments away from closed shells, rather than even-Z-even-N fragments) to that obtained from gamma-ray studies, and have application to the modeling of nuclear reactors and accelerator driven systems as a component of the total energy emitted in fission.

We are grateful to A. Sonzogni of the NNDC, Brookhaven National Laboratory for providing formatted NUDAT data for internal conversion coefficients for the full set of nuclides. The authors wish to acknowledge the role of John A. Becker in the development of GEANIE and in particular in the selection of the planar Ge detectors that were essential for this measurement. This work was performed under the auspices of an agreement between CEA/DAM and NNSA/DP on cooperation on fundamental science. Portions of this work were performed under the auspices of the U.S. Department of Energy by Los Alamos National Security, LLC, Los Alamos National Laboratory under Contract No. DE-AC52-06NA25396, and by the Lawrence Livermore National Security, LLC, Lawrence Livermore National Laboratory under Contract No. DE-AC52-07NA27344. This work has benefited from the use of the Los Alamos Neutron Science Center at LANL. This facility is funded by the U.S. Department of Energy under Contract No. DE-AC52-06NA25396.

References

1. H. Nifenecker, C. Signarbieux, M. Ribrag, J. Poitou, J. Matuszek, Nucl. Phys. A **189**, 285 (1972).
2. F. Pleasanton, R.L. Ferguson, H.W. Schmidt, Phys. Rev. C **6**, 1023 (1972).
3. F. Pleasanton, Nucl. Phys. A **213**, 413 (1973).
4. W. Reisdorf, J.P. Unik, H.C. Griffin, L.E. Glendenin, Nucl. Phys. A **177**, 337 (1971).
5. W. Younes *et al.*, Phys. Rev. C **64**, 054613 (2001).
6. T. Ethvignot, T. Granier, P. Casoli, R.O. Nelson *et al.*, *Intermediate-energy neutron-induced fission of uranium: fragment yields and isomer studies*, in *International Conference on Nuclear Data for Science and Technology 2001, 17-21 October, 2001, Tsukuba, Japan*, edited by K. Shibata (Atomic Energy Society of Japan, 2002) pp. 254–257, LA-UR-00-6031.
7. P. Casoli, Thèse de doctorat (Doctoral thesis), Université de Bordeaux, France (2003).
8. *Fission product yield data for the transmutation of minor actinide nuclear waste* (International Atomic Energy Agency, Vienna, 2008) Publication 1286, `http://www-nds.iaea.org/reports-new/tecdocs/sti-pub-1286.pdf`.
9. See, for example, *Accelerator-driven Systems (ADS) and Fast Reactors (FR) in Advanced Nuclear Fuel Cycle, A comparative Study*, OECD/NEA Nuclear Development Report (2012) and H. Ait Abderrahim *et al.*, *Accelerator and Target Technology for Accelerator Driven Transmutation and Energy Production*, Fermilab-FN-0907-DI, LA-UR-10-06754 (2010).
10. E. Cheifetz *et al.*, Phys. Rev. C **4**, 1913 (1971).
11. R.L. Watson *et al.*, Nucl. Phys. A **141**, 449 (1970).
12. V.V. Sklyarevskiy, D.E. Fomenko, E.P. Stepanov, JETP **5**, 184 (1957).
13. L.E. Glendenin, H.C. Griffin, Phys. Lett. **15**, 153 (1965).
14. L. Bridwell, M.E. Wyman, B.W. Wehring, Phys. Rev. **145**, 963 (1966).
15. A.G. Donichkin, A.N. Smirnov, V.P. Eismont, At. Energ. **41**, 329 (1976).
16. A.G. Donichkin, A.N. Smirnov, V.P. Eismont, Sov. J. Nucl. Phys. **25**, 19 (1977).
17. H.C. Griffin, J. Radioanal. Nucl. Chem. **142**, 279 (1990).
18. T. Ethvignot *et al.*, Phys. Lett. B **575**, 221 (2003).
19. T. Ethvignot *et al.*, Phys. Rev. Lett. **94**, 052701 (2005).

20. T. Ethvignot *et al.*, Phys. Rev. Lett. **101**, 039202 (2008).
21. P.W. Lisowski *et al.*, Nucl. Sci. Eng. **106**, 208 (1990).
22. P.W. Lisowski, K.F. Schoenberg, Nucl. Instrum. Methods A **562**, 910 (2006).
23. R. Nelson *et al.*, in *Proceedings of the International Conference on Nuclear Data for Science and Technology, Trieste, Italy (1997)*, edited by G. Reffo, A. Ventura, C. Granoi (SIF, Italian Physical Society, 1997).
24. N. Fotiades *et al.*, Phys. Rev. C **69**, 024601 (2004).
25. C.H. Theisen *et al.*, *SAPhIR: a fission-fragments detector*, in *Proceedings of the Second International Workshop on Nuclear Fission and Fission-Product Spectroscopy, Seyssins, France, 22-25 April 1998*, edited by G. Fioni (AIP, New York, NY, 1998) pp. 143–150.
26. T. Ethvignot, T. Granier, L. Giot, P. Casoli, R.O. Nelson, Nucl. Instrum. Methods A **490**, 559 (2002).
27. J.L. Campbell, T. Papp, At. Data Nucl. Data Tables **77**, 36 (2001).
28. J. Briesmeister (Editor), *MCNP-a general monte carlo code for neutron and photon transport*, Los Alamos National Laboratory, Report LA13709-M, Version 4C (2000).
29. A. Thompson *et al.*, *X-ray data booklet*, LBNL/PUB-490 Rev. 2 (2001).
30. K. Debertin, R.G. Helmer, *Gamma- and X-ray spectrometry with semiconductor detectors* (North-Holland, Amsterdam, 2001).
31. *PAW, Physics Analysis Workstation*, CERN program Library Long Writeup Q121 (1992).
32. F. James and M. Winkler, *MINUIT, Function minimization and Error Analysis*, CERN Program Library Long Writeup D506 (2004).
33. W. Westmeier, Nucl. Instrum. Methods **180**, 205 (1981).
34. W. Westmeier, Appl. Radiat. Isot. **43**, 305 (1992).
35. J.S. Hansen *et al.*, Nucl. Instrum. Methods **106**, 365 (1973).
36. A.C. Wahl, *Systematics of fission product yields*, Los Alamos National Laboratory Report, LA-13928 (2002).
37. Nudat 2.6, Brookhaven National Laboratory (2011).
38. A.C. Wahl, CYFP.FOR (EXE), Los Alamos National Laboratory Computer Code, LA-CC-02-0023 (2002).
39. R. Mills, *UKFY4.1: A set of prototype fission product yield library for neutron, proton, deuteron, alpha particle and spontaneous fission, developped from UKFY4.0*, JEF/DOC-1232, UKNSF(2008)P227 NDA1648.3/06/10/15 (NDATA/07-08/3/out/24) (2008).
40. W. Bambynek, *A New Evaluation of K-Shell Fluorescence Yields (Fit: K: $5 \leq Z \leq 25$)*, in *X-84 Proceedings, X-Ray and Inner-Shell Processes in Atoms, Molecules and Solids, Leipzig Aug. 20-23, 1984*, edited by A. Meisel, VEB Druckerei, Thomas Mŭnzer (Langensalza, 1984) P-1, as listed in J.H. Hubbell *et al.*, J. Phys. Chem. Ref. Data **23**, 339 (1994).
41. D. Madland, Nucl. Phys. A **772**, 113 (2006).
42. C.M. Zoller, A Gavron, J.P. Lestone *et al.*, in *Proceedings of the Seminar on Fission, Pont d'Oye III*, Vol. **56** (1995) and in *Proceedings of the VII School on Neutron Physics, Dubna*, Vol. **1** (1995) p. 130.
43. K-H Schmidt, B. Jurado, JEF/DOC 1423, OECD/NEA (2012)
44. B. Becker, P. Talou, T. Kawano, Y. Danon, J. Stetcu, Phys. Rev. C **87**, 014617 (2013).
45. D. Reignier, O. Litaize, O. Sérot, Phys. Proc. **31**, 51 (2012).
46. K.-H. Schmidt, B. Jurado, Phys. Proc. **31**, 147 (2012).
47. A. Tudora, C. Moranu, F.-J. Hambsch, Phys. Proc. **31**, 43 (2012).
48. R. Vogt, J. Randrup, D.A. Brown, M.A. Descalle, W.E. Ormand, Phys. Rev. C **85**, 024608 (2012).
49. H. Faust, Phys. Proc. **31**, 22 (2012).